

Parallel, adaptive multigrid methods for parabolic PDEs and applications

Feng Wei Yang

Department of Mathematics
University of Sussex



The Leverhulme Trust

F.W.Yang@sussex.ac.uk

25 January 2016

To solve complex non-linear parabolic systems by applying:

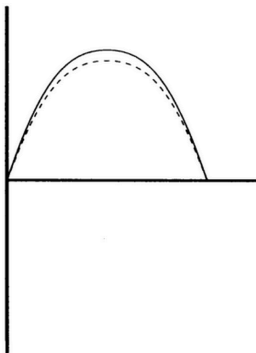
- 2^{nd} order central Finite Difference Method (FDM)
- 2^{nd} order Backward Differentiation Formula (BDF2)
- Nonlinear multigrid method with Full Approximation Scheme (FAS)
- Adaptive Mesh Refinement (AMR)
- Adaptive time-stepping
- Parallel techniques

- Multigrid methods
 - Linear multigrid
 - Nonlinear multigrid
- Thin film models from Gaskell et al. and Validation
- Tumour modelling and a model from Wise et al.
- Optimal control for whole cell tracking

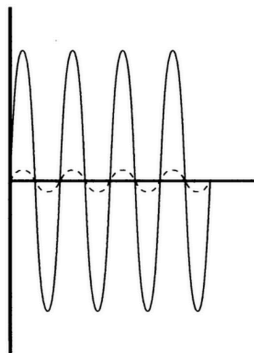
Jacobi/Gauss-Seidel iterative methods

- Well-known methods
- Require diagonally-dominant matrices
- Typically have complexity of $\mathcal{O}(n^2)$ for general sparse matrices
- ...
- Smoothing property

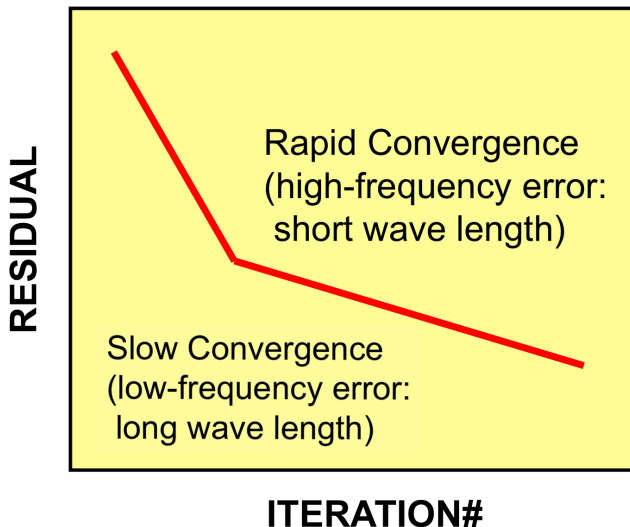
Low frequency of error



High frequency of error

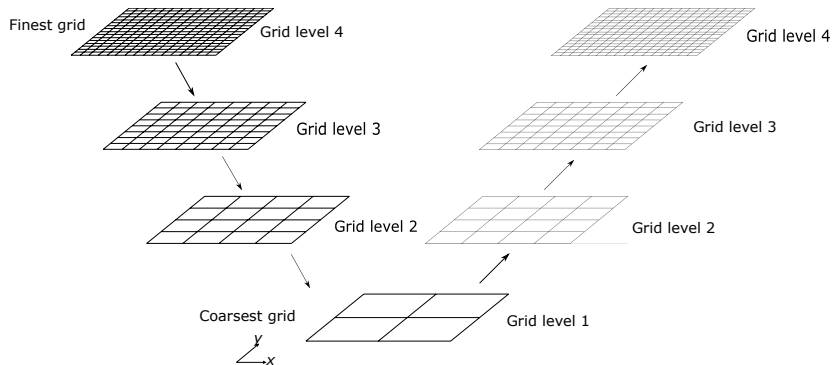


Convergence of a typical Jacobi iterative method



source: nkl.cc.u-tokyo.ac.jp

Multigrid V-cycle



Linear multigrid

A linear problem:

$$Au = b, \quad (1)$$

exact error can be obtained as

$$E = u - v, \quad (2)$$

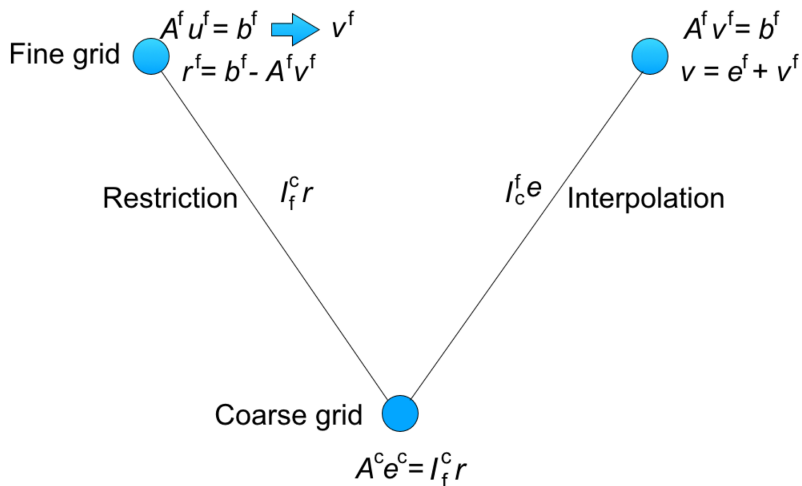
residual can be calculated as:

$$r = b - Av. \quad (3)$$

Error equation:

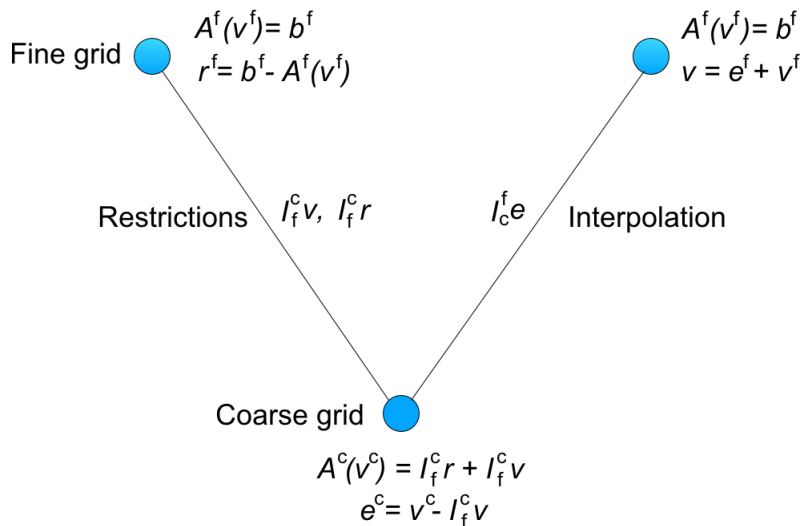
$$\begin{aligned} AE &= A(u - v) \\ &= Au - Av \\ &= b - Av \\ &= r. \end{aligned} \quad (4)$$

Linear multigrid



- The Error Equation (4) does not exist in a nonlinear case
- Full Approximate Scheme (FAS)
- For problem on coarser grids, a modified RHS is included

Nonlinear multigrid



A nonlinear point-wise smoother

Let's consider our nonlinear problem:

$$A(v) = f.$$

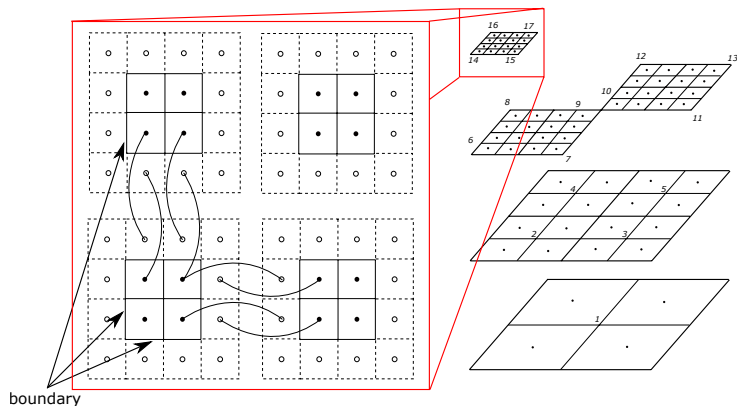
It can be rewritten as:

$$\mathcal{F}(v) = 0.$$

Then the Newton-like nonlinear point-wise smoother at a particular grid point $(i, j) \in \Omega$ can be the following:

$$v_{i,j}^{\ell+1,t+1} = v_{i,j}^{\ell,t+1} - \frac{\mathcal{F}(v)}{\mathcal{F}'(v_{i,j}^{\ell,t+1})}.$$

Domain decomposition and guard cells

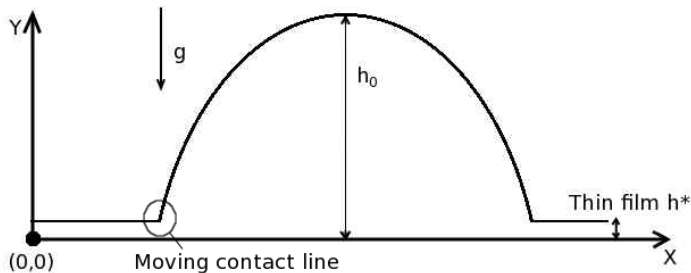


Droplet spreading model

$$\frac{\partial h}{\partial t} = \frac{\partial}{\partial x} \left[\frac{h^3}{3} \left(\frac{\partial p}{\partial x} - \frac{B_o}{\epsilon} \sin \alpha \right) \right] + \frac{\partial}{\partial y} \left[\frac{h^3}{3} \left(\frac{\partial p}{\partial y} \right) \right]$$
$$p = -\Delta(h) - \Pi(h) + B_o h \cos \alpha$$

with Neumann boundary conditions:

$$\partial_n h = 0 \quad \partial_n p = 0 \quad \text{on } \partial\Omega$$



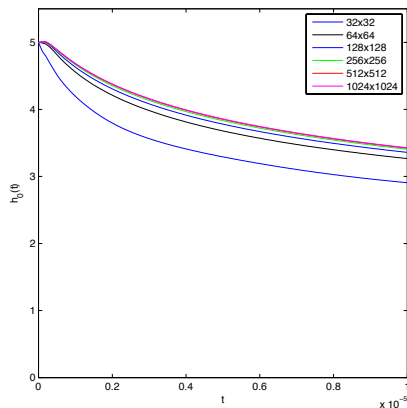
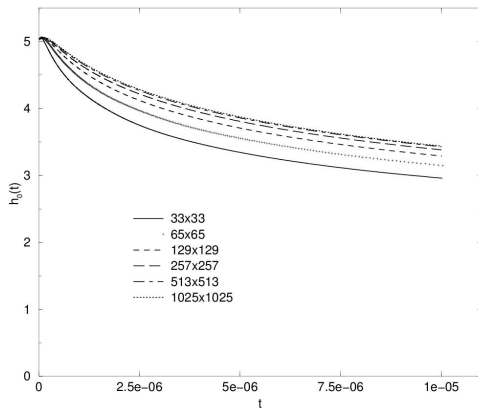
Gaskell et al. *Int. J. Numer. Meth. Fluids*, 45:1161-1186, 2004

- Cell-centred 2nd order finite difference method
- PARAMESH library for mesh generation and AMR
- Fully implicit BDF2 method with adaptive time-stepping
- MLAT variation of FAS multigrid at each time-step
- Newton-block 2×2 Red-Black (weighted) Gauss-Seidel smoother
- Full weighting restriction and bilinear interpolation
- Parallelism achieved using MPI

Update at a grid point (i, j) :

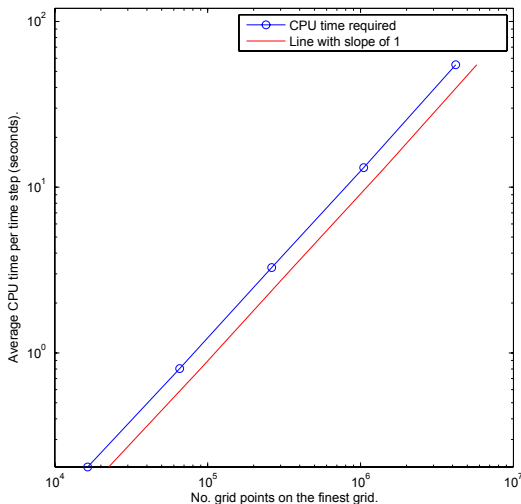
$$\begin{pmatrix} h^{\ell+1, t+1} \\ p^{\ell+1, t+1} \end{pmatrix}_{i,j} = \begin{pmatrix} h^{\ell, t+1} \\ p^{\ell, t+1} \end{pmatrix}_{i,j} - \begin{pmatrix} \frac{\partial \mathcal{F}_h}{\partial h_{i,j}^{t+1}} & \frac{\partial \mathcal{F}_h}{\partial p_{i,j}^{t+1}} \\ \frac{\partial \mathcal{F}_p}{\partial h_{i,j}^{t+1}} & \frac{\partial \mathcal{F}_p}{\partial p_{i,j}^{t+1}} \end{pmatrix}^{-1} \begin{pmatrix} \mathcal{F}_{h \ i,j}(h, p) \\ \mathcal{F}_{p \ i,j}(h, p) \end{pmatrix}$$

Validation



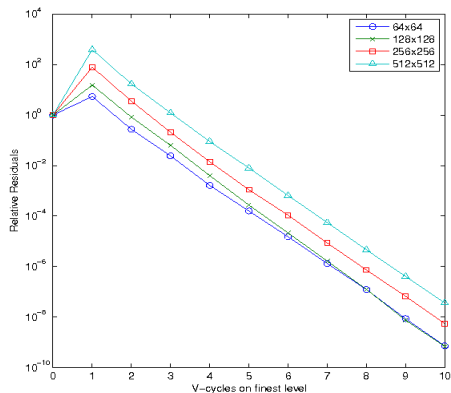
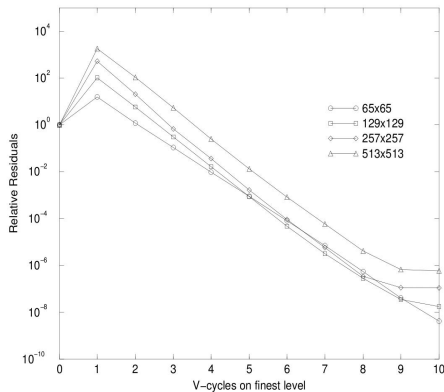
Results from Gaskell et al. on the left and our results on the right.

Multigrid linear complexity

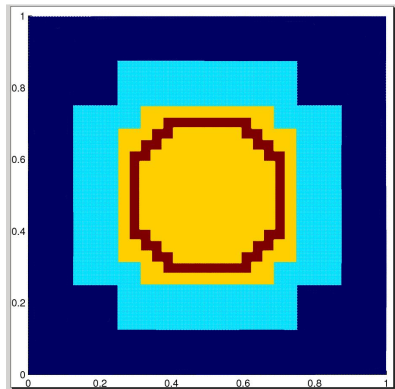
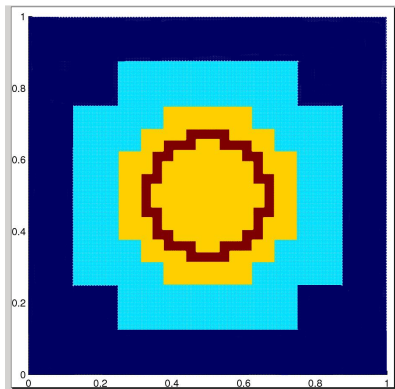


A log-log plot demonstrating the linear complexity of multigrid.

Multigrid performance

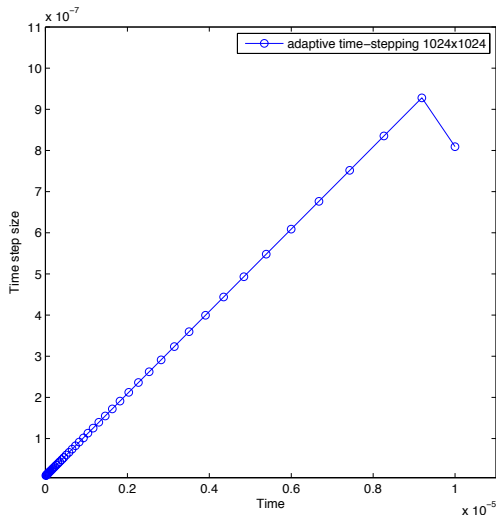


Results from Gaskell et al. on the left and our results on the right.



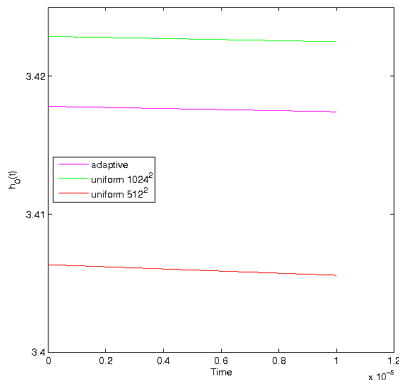
AMR with initial condition on the left and final solution on the right.

Adaptive time-stepping



Evolution of δt during $T = [0, 1 \times 10^{-5}]$.

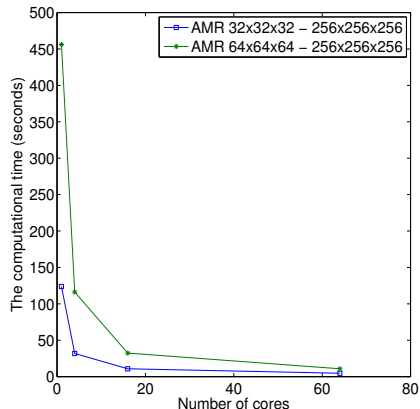
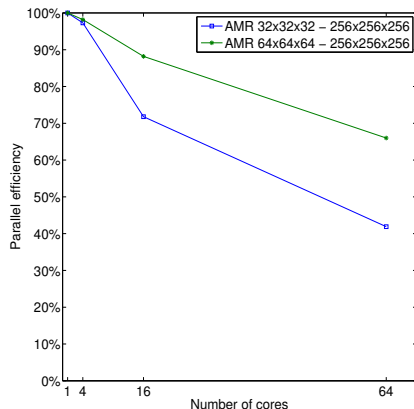
Adaptive multigrid solver



Cases	No. leaf nodes
Uniform 1024 ²	1,048,576
AMR	168,480

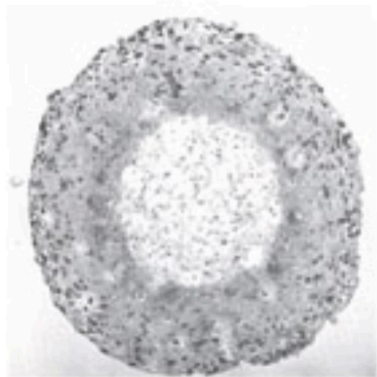
Cases	No. time steps	CPU time (seconds)
Fixed δt	1000	16721.3
ATS	45	574.4

Parallel efficiency vs. Actual computational time



Tumour modelling - avascular tumour growth

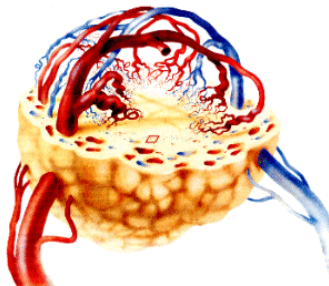
- Starts with a small cluster of cells
- Nutrient supply through diffusion
- Internal adhesion force
- Three layers of cells:
 - Proliferative cells
 - Dormant cells
 - Dead cells (necrosis)
- Volume loss in necrotic core



source: www.bioinfo.de

Tumour modelling - vascular tumour growth

- TAF chemical factor
- Inducing blood vessel (angiogenesis)
- Exponential growth rate
- Develop secondaries through metastasis



source: www.maths.dundee.ac.uk

Tumour model from Wise et al.

$$\begin{aligned}\partial_t \phi_T &= M \nabla \cdot (\phi_T \nabla \mu) + S_T(\phi_T, \phi_D, n) - \nabla \cdot (\mathbf{u}_S \phi_T) \\ \mu &= f'(\phi_T) - \epsilon^2 \Delta \phi_T \\ \partial_t \phi_D &= M \nabla \cdot (\phi_D \nabla \mu) + S_D(\phi_T, \phi_D, n) - \nabla \cdot (\mathbf{u}_S \phi_D) \\ \mathbf{u}_S &= -(\nabla p - \frac{\gamma}{\epsilon} \mu \nabla \phi_T) \\ \nabla \cdot \mathbf{u}_S &= S_T(\phi_T, \phi_D, n) \\ 0 &= \Delta n + T_C(\phi_T, n) - n(\phi_T - \phi_D)\end{aligned}$$

with mixed boundary conditions:

$$\mu = p = 0 \quad n = 1 \quad \partial_n \phi_T = \partial_n \phi_D = 0 \quad \text{on } \partial\Omega,$$

S. M. Wise, J. S. Lowengrub, V. Cristini,

Math. Comput. Modelling, 53: 1-20, 2011.

Tumour model from Wise et al.

$$\begin{aligned}\partial_t \phi_T &= M \nabla \cdot (\phi_T \nabla \mu) + S_T(\phi_T, \phi_D, n) - \nabla \cdot (\mathbf{u}_S \phi_T) \\ \mu &= f'(\phi_T) - \epsilon^2 \Delta \phi_T \\ \partial_t \phi_D &= M \nabla \cdot (\phi_D \nabla \mu) + S_D(\phi_T, \phi_D, n) - \nabla \cdot (\mathbf{u}_S \phi_D) \\ [\mathbf{u}_S &= -(\nabla p - \frac{\gamma}{\epsilon} \mu \nabla \phi_T)] \\ -\Delta p &= S_T(\phi_T, \phi_D, n) - \nabla \cdot (\frac{\gamma}{\epsilon} \mu \nabla \phi_T) \\ 0 &= \Delta n + T_C(\phi_T, n) - n(\phi_T - \phi_D)\end{aligned}$$

with mixed boundary conditions:

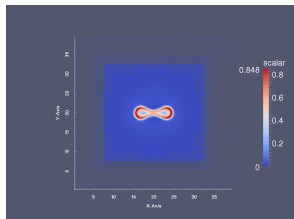
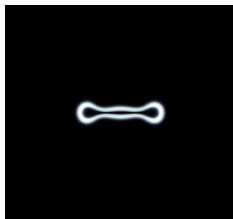
$$\mu = p = 0 \quad n = 1 \quad \partial_n \phi_T = \partial_n \phi_D = 0 \quad \text{on } \partial\Omega,$$

S. M. Wise, J. S. Lowengrub, V. Cristini,

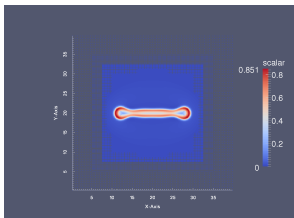
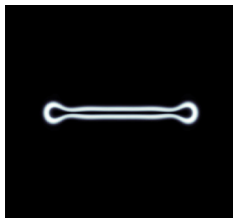
Math. Comput. Modelling, 53: 1-20, 2011.

Validation

$t=100$



$t=200$



Validation between results of Wise et al. and ours.

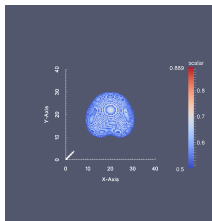
2^{nd} order convergence rate

For variable ϕ_T					
Levels	Time steps	Infinity norm	Ratio	Two norm	Ratio
5(128^2)	1250	-	-	-	-
6(256^2)	2500	9.118×10^{-2}	-	7.836×10^{-3}	-
7(512^2)	5000	1.322×10^{-2}	6.90	1.131×10^{-3}	6.93
8(1024^2)	10000	2.579×10^{-3}	5.13	2.367×10^{-4}	4.78
9(2048^2)	20000	6.415×10^{-4}	4.02	5.833×10^{-5}	4.06

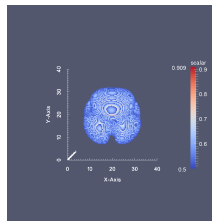
2^{nd} order convergence rate seen from the model of tumour growth.

3-D results

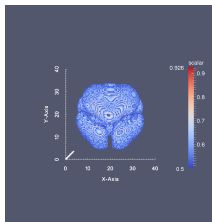
$t=50$



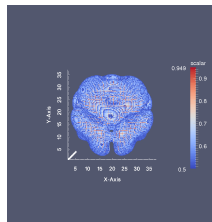
$t=100$



$t=150$

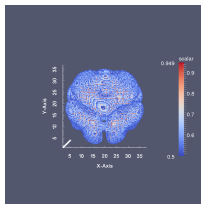


$t=200$

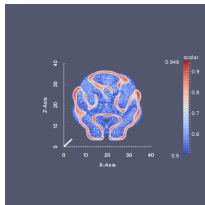


3-D results

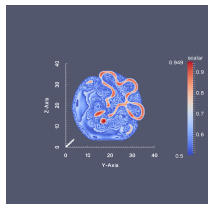
$t=200$



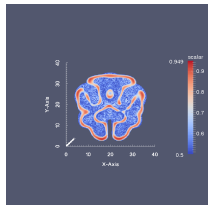
*Cutting through
y plane*



*Cutting through
x plane*

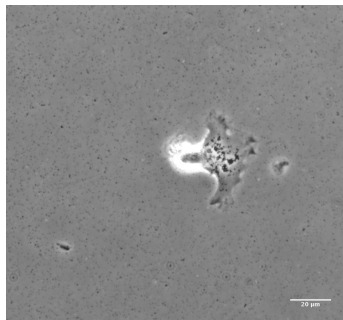
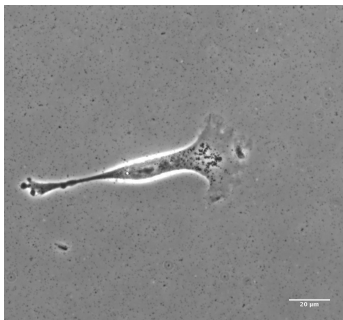


*Cutting through
z plane*



Model objectives

To track the morphology of cells and reconstruct their movements:



V. Peschetola et al. *Cytoskeleton*, 2013

What is our signature

Particle tracking:

- The morphology of cells are not considered
- Manually tracking is slow
- Automatic tracking algorithms are often flawed
 - Segmentation is suboptimal for real data
 - Tracking through pattern recognition is challenging

Pure geometric math models:

- Resolution of the data matters
- Typically no cell-setting is considered
- It is a complicated procedure to obtain the results
- Computational power and advanced numerical methods have to be included for 3-D real-life cell tracking

Our optimal control model

The volume constrained mean curvature flow with forcing:

$$\begin{cases} \mathbf{V}(\mathbf{x}, t) &= (-\sigma H(\mathbf{x}, t) + \eta(\mathbf{x}, t) + \lambda_V(t)) \mathbf{v}(\mathbf{x}, t) \text{ on } \Gamma(t), t \in (0, T], \\ \Gamma(0) &= \Gamma^0. \end{cases}$$

The phase-field approximation of the above equation - Allen-Cahn:

$$\begin{cases} \partial_t \phi(\mathbf{x}, t) &= \Delta \phi(\mathbf{x}, t) - \frac{1}{\epsilon^2} G'(\phi(\mathbf{x}, t)) - \frac{1}{\epsilon} (\eta(\mathbf{x}, t) - \lambda(t)) \text{ in } \Omega \times (0, T], \\ \nabla \phi \cdot \boldsymbol{\nu}_\Omega &= 0 \text{ on } \partial\Omega \times (0, T], \\ \phi(\cdot, 0) &= \phi^0 \text{ in } \Omega. \end{cases}$$

Our optimal control model cont.

The objective functional:

$$J(\phi, \eta) = \frac{1}{2} \int_{\Omega} (\phi(\mathbf{x}, T) - \phi_{obs}(\mathbf{x}))^2 d\mathbf{x} + \frac{\theta}{2} \int_0^T \int_{\Omega} \eta(\mathbf{x}, t)^2 d\mathbf{x} dt,$$

and now we solve the minimisation problem:

$$\min_{\eta} J(\phi, \eta), \text{ with } J \text{ given above.}$$

Our optimal control model cont.

The adjoint equation to help computing the derivative of the objective functional:

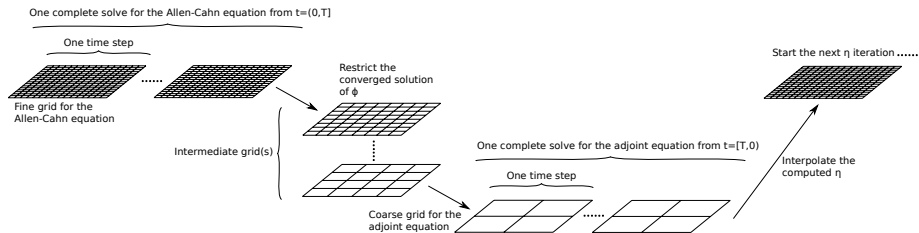
$$\begin{cases} \partial_t p(\mathbf{x}, t) = -\Delta p(\mathbf{x}, t) + \epsilon^{-2} G''(\phi(\mathbf{x}, t)) p(\mathbf{x}, t) & \text{in } \Omega \times [0, T), \\ p(\mathbf{x}, T) = \phi(\mathbf{x}, T) - \phi_{obs}(\mathbf{x}) & \text{in } \Omega, \end{cases}$$

and we update the control as

$$\eta^{\ell+1} = \eta^\ell - \alpha \left(\theta \eta^\ell + \frac{1}{\epsilon} p^\ell \right).$$

- Number of time steps
- Memory requirement (let's consider double precision and 100 time steps)
 - 2-D: 512^2 requires 0.4 gigabytes
 - 3-D: 512^3 requires 215 gigabytes

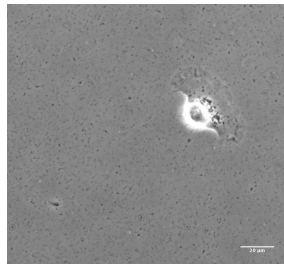
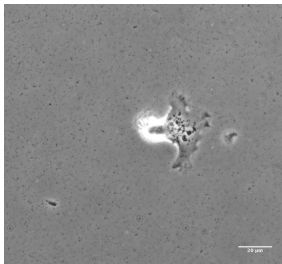
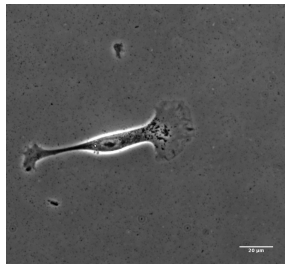
Two-grid solution strategy



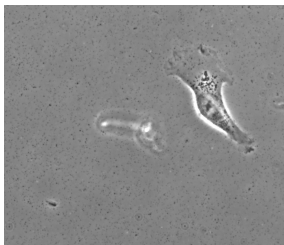
Real world example (1)

Real world example (1)

$t=0$



$t=T$



Real world example (1)

Real world example (2)

Euler number for topological changes

We compute this Euler number for these time steps with an "optimized" control η :

$$\mathcal{X} = \frac{1}{2\pi(a-b)} \int_{\Omega(a,b)} \left(-\Delta\phi + \frac{\nabla|\nabla\phi|^2 \cdot \nabla\phi}{2|\nabla\phi|^2} \right) dx.$$

Q. Du et al. *J. Appl. Math.*, 2005

Real world example (2)

A 3-D example

F.W. Yang, C.E. Goodyer, M.E. Hubbard and P.K. Jimack

"An Optimally Efficient Technique for the Solution of Systems of Nonlinear Parabolic Partial Differential Equations"

AiES in review, 2015

F. Yang, C. Venkataraman, V. Styles and A. Madzvamuse

"A Robust and Efficient Adaptive Multigrid Solver for the Optimal Control of Phase Field Formulations of Geometric Evolution Laws"

CiCP in review, 2015

F. Yang, C. Venkataraman, V. Styles, V. Kutenberger, E. Horn, Z. von Guttenberg and A. Madzvamuse

"A Computational Framework for Particle and Whole Cell Tracking Applied to a Real Biological Dataset"

JBM in review, 2015